Biophysical Chemistry 159 (2011) 24–32

Contents lists available at ScienceDirect

Biophysical Chemistry

journal homepage: http://www.elsevier.com/locate/biophyschem

From steroid receptors to cytokines: The thermodynamics of self-associating systems

Keith D. Connaghan [a], Amie D. Moody [a], James P. Robblee [a], James R. Lambert [b], David L. Bain [a,*]

[a] Department of Pharmaceutical Sciences, University of Colorado Anschutz Medical Campus, Aurora, CO 80045, United States
[b] Department of Pathology, University of Colorado Anschutz Medical Campus, Aurora, CO 80045, United States

ARTICLE INFO

Article history:
Received 31 March 2011
Received in revised form 19 April 2011
Accepted 19 April 2011
Available online 27 April 2011

Keywords:
Protein–DNA interaction
Thermodynamics
Gene regulation
Steroid receptor
Cytokine

ABSTRACT

Since 1987, the Gibbs Conference on Biothermodynamics has maintained a focus on understanding the quantitative aspects of gene regulatory systems. These studies coupled rigorous techniques with exact theory to dissect the linked reactions associated with bacterial and lower eukaryotic gene regulation. However, only in the last ten years has it become possible to apply this approach to clinically relevant, human gene regulatory systems. Here we summarize our work on the thermodynamics of human steroid receptors and their interactions with multi-site promoter sequences, highlighting results not available from more traditional biochemical and structural approaches. Noting that the Gibbs Conference has also served as a vehicle to promote the broader use of thermodynamics in understanding biology, we then discuss collaborative work on the hydrodynamics of a cytokine implicated in tumor suppression, prostate derived factor (PDF).

1. Introduction

A major focus of the Gibbs Conference on Biothermodynamics has been on the quantitative aspects of gene regulatory systems. In the early years of the meeting, this focus extended to studies of bacterial DNA binding proteins such as biotin [1] and cytidine repressors [2], or yeast proteins such as TATA binding protein [3]. By contrast, little work was presented on higher eukaryotic transcription factors such as the human steroid receptors. This was in part because the biochemical framework for understanding steroid receptor function – the "wiring diagram" – was still unclear. Moreover, it was not yet possible to recombinantly express and purify high molecular weight, human transcription factors.

Due to a number of advances in the 1990s, this situation began to change dramatically. First, new contributors to steroid receptor-mediated gene regulation (e.g. coactivators) were identified and characterized. Second, the high-resolution structures of steroid receptor domains became available. Third, cellular assays allowed the functional characterization and analysis of receptor–promoter interactions. Finally, it became possible to express and purify milligram amounts of receptors using baculovirus–insect cell expression systems. These advances allowed researchers such as us to initiate thermodynamic studies of receptor–promoter interactions to determine the "rules and states" associated with steroid receptor function.

Our objective has been to determine the functional energetics of receptor assembly at multi-site promoter sequences, and correlate these results to cellular outcomes. In light of groundbreaking work on systems such as the λ repressor–right operator [4], we have focused on microscopic interaction parameters, especially those of receptor self-association and inter-site cooperativity. We have also stressed the importance of rigorous techniques and exact theory — topics that have been featured prominently at the Gibbs Conference. In the first half of this review, we highlight our recent work on the microstate thermodynamics of steroid receptor behavior, emphasizing results and implications not available from more traditional biochemical and structural approaches.

Finally, noting that thermodynamic dissections cannot account for the entirety of receptor function, we initiated a collaboration with coauthor James Lambert, a biochemist and molecular biologist with a long-standing interest in steroid receptor action. Our initial goal was to determine the extent to which our thermodynamic results might translate into cell-based function. However, in the course of our conversations, we discovered another area of mutual interest: transforming growth factor (TGF)-β cytokines and their role in prostate cancer. Noting that an additional focus of the Gibbs Conference has been to "develop and foster [a] broader vision of what thermodynamics has to offer in the study of biological systems" [5], we initiated a study to address the quantitative aspects of the TGF-β cytokine, prostate derived factor (PDF). We summarize the results of this work in the second half of this review.

2. Unresolved issues in steroid receptor function

Steroid receptors are ligand-activated transcription factors. The family comprised the androgen receptor (AR), estrogen receptor (ER), glucocorticoid receptor (GR), mineralocorticoid receptor (MR) and

* Corresponding author at: Department of Pharmaceutical Sciences, C-238, University of Colorado Anschutz Medical Campus, 12850 E. Montview Blvd, Aurora, CO 80045, United States. Tel.: +1 303 724 6118; fax: +1 303 724 7266.
E-mail address: David.Bain@ucdenver.edu (D.L. Bain).

0301-4622/$ – see front matter © 2011 Elsevier B.V. All rights reserved.
doi:10.1016/j.bpc.2011.04.013

progesterone receptor (PR). PR exists naturally as two isoforms (PR-A and PR-B) as does ER (ER-α and ER-β.) The receptors are structurally homologous, particularly via their highly conserved DNA binding domains (DBDs). Not surprisingly then, *in vitro* the receptors recognize and bind to largely identical DNA response elements and can transcriptionally activate identical genes. Yet *in vivo*, the proteins have largely non-overlapping roles in regulating metabolism, puberty, inflammation, water balance and pregnancy. These differences arise by the ability of the receptors to activate different gene networks.

All the receptors share a common modular structure, as shown in Fig. 1. Centrally located is the highly conserved DBD; C-terminal to the DBD is a hormone binding domain linked via a short hinge sequence. The N-terminal region is highly variable in size and sequence, but shares the common attribute of being natively disordered. Finally, both the N-terminal and C-terminal sequences contain transcriptional activation functions (AFs). The biochemically-based model of steroid receptor function posits that unactivated steroid receptors are located predominantly in the cytoplasm. Steroidal hormone binding is coupled to release of heat-shock proteins, receptor dimerization and translocation into the nucleus. Receptor dimers then bind to palindromic hormone response elements (HREs) located within receptor-regulated promoters, and activate gene expression via coactivator recruitment and interaction with the general transcriptional machinery [6].

Close consideration of the above model reveals some limitations and unanswered questions. For example, if steroid receptors bind identical binding sites and with similar apparent binding affinities, then how do they regulate different genes? This question is not a new one — several studies postulated that the ability of different receptors to differentially regulate a particular gene was due to their differential ability to recruit coactivators to the promoter of that gene [7,8]. Alternative explanations have included DNA as an allosteric effector [9] and combinatorial assembly of transcription factors [10].

The advent of microarray technology revealed even more complexity. These studies demonstrated that a steroid receptor could simultaneously activate hundreds of genes — and the degree of activation spanned the range from weak to strong [11]. Even more intriguing were the results of direct comparative analyses (e.g. PR versus GR), demonstrating that two different steroid receptors could activate identical genes (to similar or different transcriptional levels) while simultaneously activating different subsets of genes [12]. Likewise, comparative analyses of steroid receptor isoforms also revealed differential but overlapping gene regulation [11,13]. The standard model of steroid receptor function cannot easily account for receptor-specific gene regulation at such a widespread level.

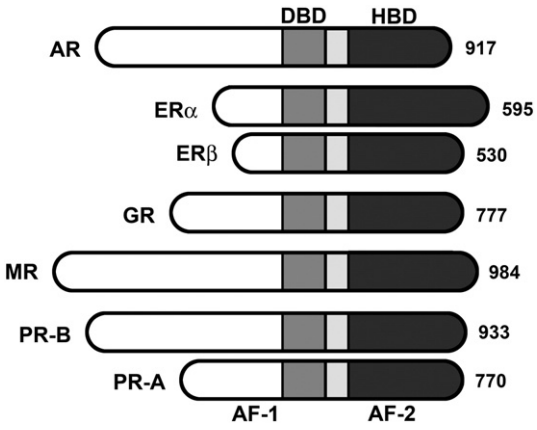

Fig. 1. Schematic representation of steroid receptor structures. Receptors are as indicated on the left; number of amino acids is shown on right. Functional regions are as indicated: DBD, DNA binding domain; HBD, hormone binding domain; activation function, AF.

There are a number of reasons why receptor-specific gene regulation is not well understood. First, nearly every study of steroid receptor–DNA interactions has measured an apparent binding constant. Just as in measuring a K_m, it is impossible to determine mechanism from such a macroscopic parameter. Second, much of the research that has led to our current model of function was carried out with techniques or analyses we now know to be of limited utility — Scatchard analysis, filter binding, charcoal adsorption and gel shift assays, for example. Third, receptors were only partially purified or of unknown functional activity. Finally, most studies have focused on a single receptor rather than on the interactions among receptors. Yet the *in vivo* presence of multiple, active receptor populations is the rule rather than the exception. The two PR isoforms are a perfect example — they are naturally present at equimolar ratios, and dysregulation of this ratio is associated with breast cancer [14]. In particular, an excess of the PR-A isoform is linked to a poorer prognosis [15].

Noting that steroid receptor-regulated promoters typically contain multiple hormone response elements, we initially hypothesized that receptor-specific differences in inter-site cooperativity might account for differences in receptor-specific promoter activation. Differences in cooperativity would dictate the degree of successful promoter occupancy when different receptors competed for identical binding sites — similar cooperative binding energetics would result in jointly regulated genes whereas differential cooperativity would generate receptor-specific gene regulation. We used analytical ultracentrifugation and quantitative footprinting to test this hypothesis, specifically by dissecting and isolating the microscopic energetics of receptor–promoter binding.

3. Thermodynamic dissection of progesterone receptor–promoter interactions

Shown in Fig. 2 is a schematic representation of receptor binding to a simple two-site promoter sequence (HRE_2). Also shown are the relevant microscopic binding parameters. Receptor monomers dimerize in solution with a dimerization constant of k_{dimer}. A preformed dimer then binds at a palindromic HRE with intrinsic affinity of k_{int}. Receptor dimer binding at the remaining palindrome results in inter-site cooperativity, k_c. We first present a comparative analysis of PR isoform interactions at the HRE_2 promoter, focusing on the hypothesis that differences in cooperativity might account for the unique

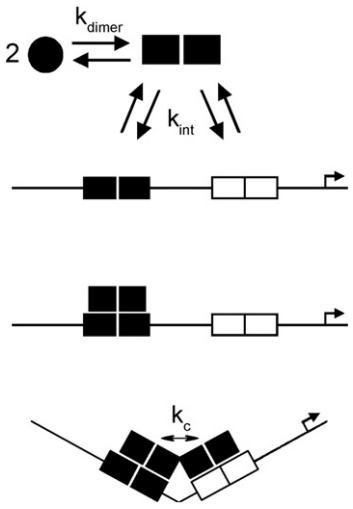

Fig. 2. Schematic representation of receptor:HRE_2 assembly states. Circles represent hormone-bound receptor monomers, squares represent dimers. Dimerization (k_{dimer}) is coupled to response element binding (k_{int}); complete occupancy is coupled to an inter-site cooperative interaction (k_c). Arrow refers to the direction of transcriptional start site.

activation profiles of each isoform. In the next section, we focus on the molecular forces responsible for cooperativity and the role of promoter layout in influencing this parameter. In Section 5, we extend our analysis to other steroid receptor family members.

The first step in dissecting receptor–promoter interactions requires an explicit evaluation of receptor self-association (k_{dimer}) in the absence of DNA. Shown in Fig. 3 are representative sedimentation equilibrium data collected for full-length, human PR-A. Three concentrations covering a ten-fold range were equilibrated at three rotor speeds. Simultaneous analysis of all nine data sets resolved a dimerization constant of 1.08 μM, corresponding to a free energy change of −7.2 kcal/mol [16]. A statistically identical result was obtained by sedimentation velocity [16], strongly indicating that PR-A monomers and dimers each represent homogeneous species. Analogous studies were carried out for the second PR isoform, PR-B. A similar result of −7.6 kcal/mol was obtained, demonstrating that under identical solution conditions, the two isoforms maintain equivalent dimerization energetics [17].

Quantitative footprinting was used to study assembly of the PR isoforms at the HRE_2 promoter. Shown in Fig. 4A is a footprint titration of PR-A binding to the promoter. It is evident that protection is specific for each of the two HREs. Shown in Fig. 4B are the resultant individual-site binding isotherms for PR-A binding to each response element and binding to a reduced-valency template containing only a single HRE (HRE_{1-}). Fig. 4C shows the results of analogous experiments for PR-B binding under identical conditions. Comparison by visual inspection suggests significantly more cooperative binding for PR-B relative to PR-A; however, a more quantitative approach is to resolve the microscopic parameters associated with cooperative binding using statistical mechanics.

Since quantitative footprinting is a thermodynamically valid technique [18], each individual-site isotherm represents the probability of all microscopic interactions associated with binding at that site. The expressions that describe each isotherm are constructed by summing the probabilities of each configuration associated with binding. The probability (f_s) of any microscopic configuration is defined as [19]:

$$f_s = \frac{\exp\left(-\Delta G_{(s)} / RT\right) \times [x]^j}{\sum_s \sum_j \exp\left(-\Delta G_{(s)} / RT\right) \times [x]^j} \quad (1)$$

where $\Delta G_{(s)}$ is the free energy of configuration state s relative to the unliganded reference state, x is equal to the free PR monomer concentration (as calculated from the dimerization constant) and j is the stoichiometry of PR monomer bound to a response element. R is the gas constant and T is temperature in Kelvin. For example, the equation representing the fractional saturation ($\overline{Y}$) for PR-A or PR-B dimer assembly at an individual site on the HRE_2 promoter is:

$$\overline{Y} = \frac{(k_{dimer} \cdot k_{int})[x]^2 + \left(k_{dimer}^2 \cdot k_{int}^2 \cdot k_c\right)[x]^4}{1 + 2(k_{dimer} \cdot k_{int})[x]^2 + (k_{dimer}^2 \cdot k_{int}^2 \cdot k_c)[x]^4} \quad (2)$$

where k_{dimer} is the dimerization dissociation constant (determined independently using sedimentation velocity and equilibrium), k_{int} is the intrinsic affinity of a PR dimer for a PRE, k_c is the intersite cooperativity, x is again equal to the free PR-A monomer concentration (as calculated from the dimerization constant). Since each HRE in the HRE_2 promoter is identical in sequence, the sites are isoenergetic and the same equation describes binding to each response element.

Using an analogous approach, the equation describing the fractional saturation of site 2 of the HRE_{1-} promoter is:

$$\overline{Y}_{1-} = \frac{(k_{dimer} \cdot k_{int}) \times [x]^2}{1 + (k_{dimer} \cdot k_{int}) \times [x]^2}. \quad (3)$$

Simultaneous fitting of all three isotherms (from either Fig. 4B or C) resolves the microscopic binding terms k_{int} and k_c. The previously determined dimerization constant, k_{dimer}, (determined under identical solution conditions) is a fixed parameter in the fitting process.

The results of the analysis for PR-A and PR-B assembly at the HRE_2 promoter are shown in Table 1. As already noted, the two isoforms maintain statistically identical dimerization energetics under these conditions. However, their DNA binding energetics are quite different. In particular, the energetics of cooperativity differ by 2.1 kcal/mol, corresponding to a 45-fold difference. Despite the fact that the receptors have identical DNA binding domains (see Fig. 1), the intrinsic binding energetics also differ, although not as dramatically as cooperativity.

The large difference in binding energetics results in a greatly increased PR-B occupancy at the HRE_2 promoter relative to PR-A. Shown in Fig. 5 are the calculated probabilities for each receptor–promoter ligation state as a function of total isoform concentration. Full saturation of the promoter by PR-B occurs at a concentration over an order of magnitude lower relative to PR-A. This difference correlates with cellular and molecular biological studies of isoform-specific function — the stronger transcriptional activation ability of PR-B relative to PR-A is consistent with the former's increased cooperative binding interactions. Since we have also observed that the ability of PR isoforms to recruit coactivators to a promoter is coupled to cooperativity [20], it may be cooperative binding rather than simply DNA binding that is the prime determinant of coactivator recruitment and therefore transcriptional activation.

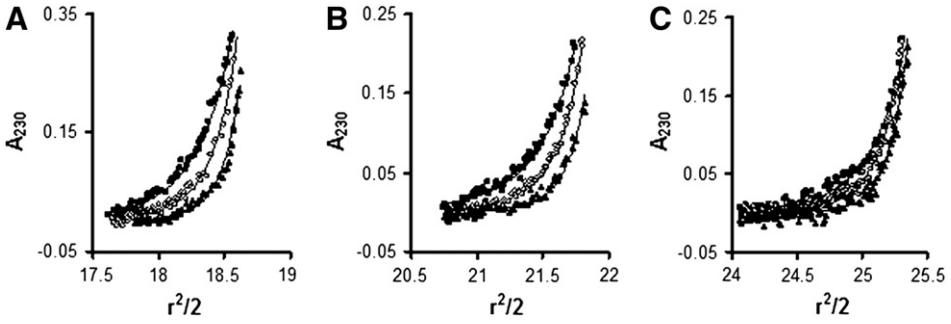

Fig. 3. Sedimentation equilibrium analysis of PR-A. Panels represent each PR-A loading concentration: (A) 1.0 μM, (B) 0.5 μM and (C) 0.25 μM. Symbols represent PR-A absorbance at 15,000 rpm (squares), 18,000 rpm (circles), and 21,000 rpm (triangles). Solid lines represent the best fit model (monomer–dimer) from simultaneous analysis of all nine data sets using the program NONLIN [42]. Square root of the variance was 0.010 absorbance units. Buffer conditions were 20 mM Hepes, pH 8.0, 300 mM NaCl, 2.5 mM $MgCl_2$, 1 mM $CaCl_2$, 1 mM DTT, and 10^{-5} M progesterone at 4 °C. Identical results were obtained for NaCl concentrations ranging from 50 mM to 1 M.

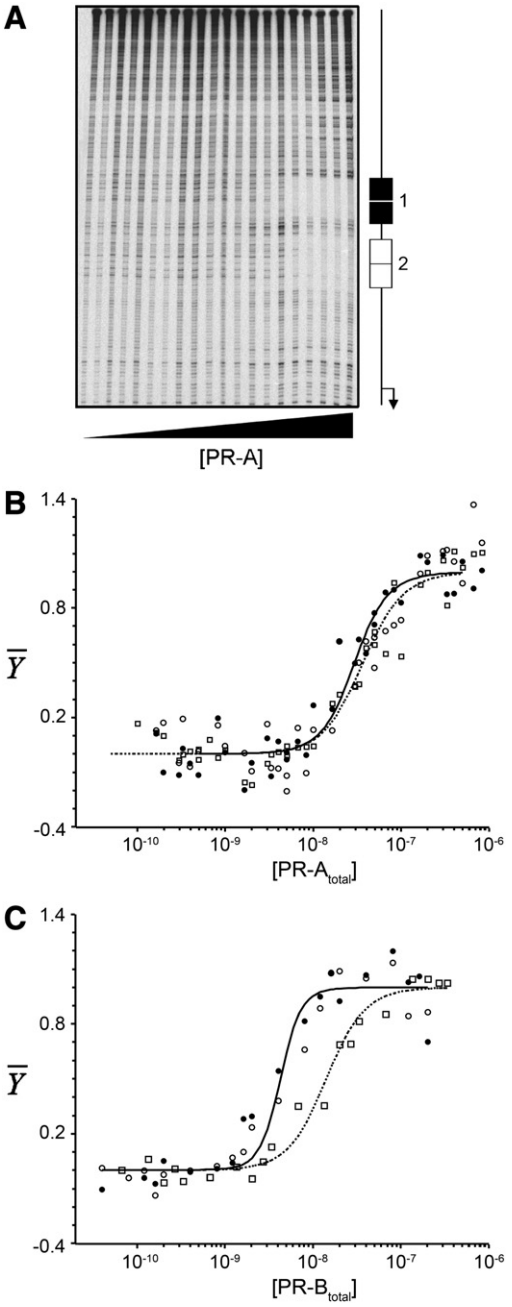

Fig. 4. Quantitative footprint titration and individual-site isotherms for PR-A and PR-B assembly at the HRE_2 promoter. (A) Representative titration of the HRE_2 promoter by PR-A. Positions of the two HREs (site 1, filled rectangle; site 2, open rectangle) are indicated to the right. (B) Individual-site isotherms for PR-A binding to site 1 (filled circles) and site 2 (open circles) of the HRE_2 promoter, and binding to site 2 (open squares) of the HRE_{1-} promoter. Lines represent best fit to all data using Eqs. (2) and (3). Buffer conditions were 20 mM Hepes, pH 8.0, 50 mM NaCl, 2.5 mM $MgCl_2$, 1 mM $CaCl_2$, 1 mM DTT, and 10^{-5} M progesterone at 4 °C. (C) Same as *B*, but PR-B individual-site isotherms are displayed.

4. Cooperativity is tunable for both isoforms

One question that arose from our studies of the HRE_2 promoter was if PR-B maintained greater cooperative binding energetics than PR-A, then how could the A-isoform regulate any gene since it would always be outcompeted for promoter binding? Simulations of competitive PR-A versus PR-B binding to the HRE_2 promoter suggested that either an increase in PR-A cooperativity or a decrease in PR-B cooperativity would allow PR-A to displace PR-B from the

Table 1
Resolved free energy changes and differences for PR-A and PR-B:PRE_2 binding interactions.[a]

Interaction Free energy	PR-A (kcal·mol^{-1})	PR-B (kcal·mol^{-1})	ΔΔG[b] (kcal·mol^{-1})
ΔG_{dimer}	-7.6 ± 0.6[c]	-7.2 ± 0.7[c]	-0.4 ± 0.9
ΔG_{int}	-11.4 ± 0.1	-12.8 ± 0.1	1.4 ± 0.1
ΔG_c	-0.4 ± 0.2	-2.5 ± 0.1	2.1 ± 0.2

[a] Values previously published [21] and determined based on the relationship $\Delta G_i = -RT\ln(k_i)$.
[b] Free energy difference for each set of parameters.
[c] Free energy change for solution dimerization measured independently using sedimentation equilibrium [16,17].

response elements [21]. Here we demonstrate that PR-A cooperativity can indeed be enhanced as a consequence of binding site layout [22]. We also demonstrate that PR-B cooperativity can be selectively decreased by changes in monovalent cation type [23].

The mouse mammary tumor virus (MMTV) promoter is one of the only natural steroid-responsive promoter gene regulatory sequences that is well characterized biochemically and structurally. The wild-type promoter contains four recognizable response elements — one palindromic site and three half-sites. As shown in Fig. 6A, quantitative footprinting using PR-A reveals protection at all four sites. (Site 5 is a cryptic site not thermodynamically linked to binding at the remaining sites.) Simultaneous analysis of seven different promoter templates, coupled to sedimentation equilibrium analysis of the protein–DNA complex, revealed the following: 1) PR-A monomers rather than

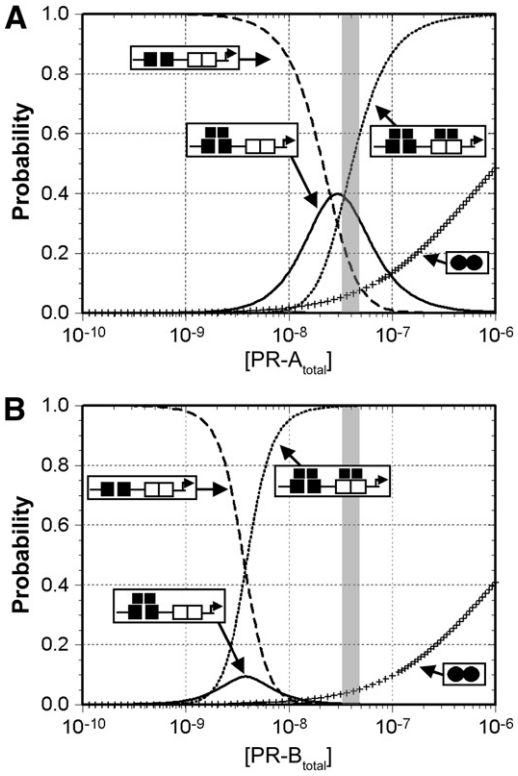

Fig. 5. Predicted distribution of each macroscopic PR-A:HRE_2 and PR-B:HRE_2 ligation state. (A) Distribution of PR-A ligation states as predicted from the experimentally determined energetics (Table 1). (B) Same as *A* except that PR-B ligation states are displayed. Unligated HRE_2 is represented by dashed line; singly ligated promoter is represented by solid line; fully ligated promoter is represented by dotted line, and proportion of free dimer is represented by "+". The shaded box represents the estimated intracellular PR concentration [43].
Figure reproduced with permission from [21]. Copyright 2007 National Academy of Sciences, USA.

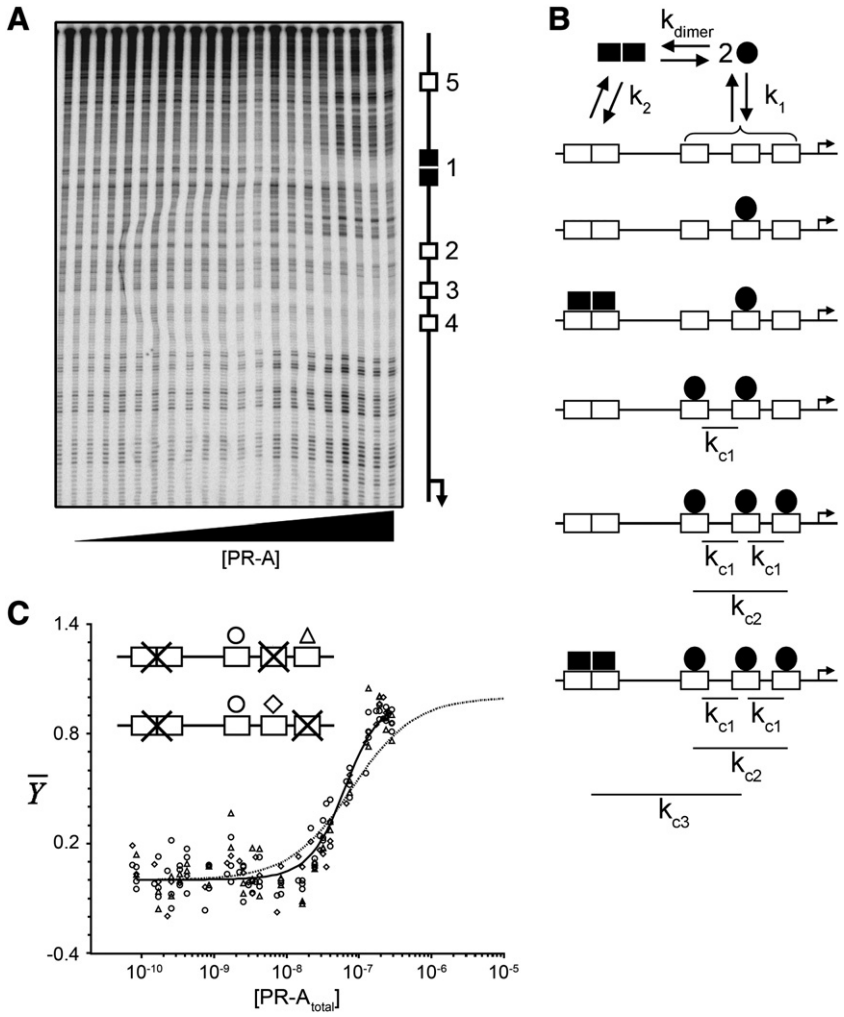

Fig. 6. Quantitative footprint titration, schematic representation of assembly states, and individual-site isotherms for PR-A binding to the MMTV promoter. (A) Representative titration of the $MMTV_{wt}$ promoter by PR-A. Positions of the HREs are shown to the right. (B) Schematic of PR-A:MMTV promoter assembly states. Monomers dimerize in solution (k_{dimer}) and bind at half-sites (k_1); dimers bind at the palindromic site (k_2). Monomers bound at half-sites cooperatively interact in a pair-wise fashion (k_{c1}). Non-additive cooperativity induced by addition of a third monomer to the half-sites is accounted for by k_{c2}. Saturation of the promoter is linked to a third cooperative interaction between the palindrome and the three half-sites (k_{c3}). (C) Individual-site isotherms for PR-A binding to the reduced-valency $MMTV_{1-,3-}$ and $MMTV_{1-,4-}$ promoters (see figure inset). Solid line represents a simultaneous fit to a pair-wise cooperative model by fixing ΔG_1 at −8.1 kcal/mol and allowing ΔG_{c1} to float. Dotted line represents a global fit to all data using a non-cooperative two-site model. Monomer binding to site 2 (open circles); binding to site 3 (open diamonds); binding to site 4 (open triangles).

dimers assemble at the three half-sites; 2) monomers bound at half-sites are capable of significant pairwise cooperative interactions; 3) occupancy of all three half-sites is required to cooperatively engage the palindromic-bound dimer; and finally, 4) large unfavorable forces accompany receptor assembly at the promoter. The binding pathway associated with these results is presented in Fig. 6B.

Shown in Fig. 6C is a representative set of individual-site binding isotherms for two of the reduced-valency templates, $MMTV_{1-,3-}$ and $MMTV_{1-,4-}$. Comparison of the experimental data and best fit curve (solid line) to a forced non-cooperative fit (dotted line) reveals clear visual evidence for cooperativity. Quantitative analysis reveals the pairwise interaction term to be −2.0 kcal/mol, which corresponds to a ~40-fold increase in PR-A binding stability. By contrast, the pairwise cooperativity for PR-A dimers at the HRE_2 promoter was only −0.9 kcal/mol, or a 5-fold increase in stability. These results provide direct evidence that promoter architecture and protomeric state can modulate PR-A cooperative interactions. Moreover, they highlight the unique insight available from this type of thermodynamic dissection: all previous studies of receptor–MMTV promoter interactions concluded that only dimers bound to the response elements, and did so with little or no cooperativity [24,25].

As discussed earlier, PR-B exhibits strong cooperative binding to the HRE_2 promoter (Fig. 4C and Table 1). The footprinting experiments that demonstrated this result were carried out in a buffer containing 50 mM Na^+. Shown in Fig. 7A is a matched study except that Na^+ has been replaced with 50 mM K^+. Note that K^+ has completely eliminated any PR-B cooperativity ($k_c = 0.5$) [23]. Moreover, as seen in Table 2, there is little effect on receptor dimerization or intrinsic DNA binding. These results suggested to us that PR-B cooperativity is allosterically regulated by a Na^+ or K^+ binding event. We explored this possibility by carrying out sedimentation velocity studies as a function of monovalent cation (M^+) type.

Shown in Fig. 7B are the results of PR-B sedimentation velocity studies as a function of the chloride salts of the Group 1a cations (LiCl, NaCl, KCl, RbCl and CsCl). Plotted are the resolved weight-average sedimentation coefficients, $\langle s_{20,w} \rangle$, for PR-B determined in these salts, and at three salt concentrations. In 50 mM MCl, the sedimentation coefficient reaches a minimum when the protein is in Na^+ but reaches maximal values when determined in the cations at the extremes of the series (Li^+ and Cs^+). When the MCl concentration is decreased to 10 mM, the sedimentation coefficient increases only slightly in Na^+ but increases significantly in the presence of Li^+, K^+ and Rb^+. We

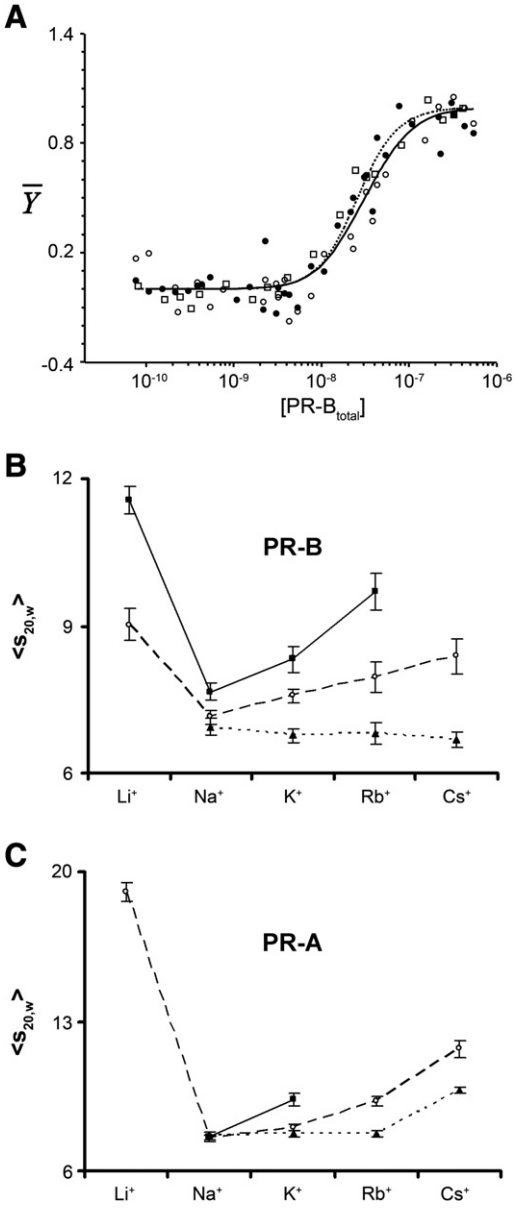

Fig. 7. Individual-site binding isotherms for PR-B binding to the HRE_2 promoter in KCl, and weight-average *s* plots for PR-B and PR-A as a function of monovalent cation type. (A) Individual-site binding isotherms for PR-B binding to site 1 (filled circles) and 2 (open circles) of the HRE_2 promoter, and site 2 (open square) of the HRE_{1-} promoter in 50 mM KCl. Lines (HRE_2, solid; HRE_{1-}, dotted) represent best fit model using Eqs. (2) and (3). (B) Initial PR-B loading concentration was 1.0 μM. The weight average sedimentation coefficient was determined as implemented in the program DCDT+ [44,45]. Error estimates represent one standard deviation as reported by DCDT+. Solution conditions minus MCl were 20 mM Tris, pH 8.0, 2.5 mM $MgCl_2$, 1 mM $CaCl_2$, 1 mM DTT, and 10^{-5} M progesterone at 4 °C. The concentration of MCl was 10 mM (squares, solid line), 50 mM (open circles, dashed line) or 300 mM (triangles, dotted line). M^+ is as indicated on the plot. (C) As described for *B* except the results for PR-A are displayed. Concentration of MCl was 100 mM (squares, solid line), 200 mM (open circles, dashed line) or 300 mM (triangles, dotted line). M^+ is as indicated on the plot.

interpret these results to mean that bulky cations like Cs^+ or highly hydrated ions like Li^+ are too large to interact at an M^+ binding site, resulting in aggregation of that receptor fraction unable to bind cation (i.e. apo-receptors).

As seen in Fig. 7C, a similar phenomenon is observed for PR-A. Again, a minimum in $\langle s_{20,w} \rangle$ is found in at Na^+ concentrations of 200 mM, with larger values seen at the extremes of the MCl series. The same qualitative result is observed at 100 mM NaCl and KCl. (Data collected in 100 mM LiCl, RbCl and CsCl were unanalyzable due to heavy precipitation.) Interestingly, when the MCl concentration is increased to 300 mM, Na^+, K^+ and Rb^+ generate the same value, suggesting that the receptor is saturated by the respective cations. Since the sedimentation coefficients for both isoforms when in KCl increase at concentrations of 50–100 mM, the K^+ binding affinity must be roughly 100 mM. Likewise, the $\langle s_{20,w} \rangle$ for at least PR-B in NaCl is unperturbed from 50 to 300 mM indicating that Na^+ binding affinity towards this isoform must be below 50 mM. Because PR-A is less soluble at low salt concentrations, we were unable to estimate Na^+ binding affinity for this isoform.

Table 2
Energetics of PR self-association and PR-B:PRE_2 binding interactions in NaCl and KCl under matched conditions.[a]

Interaction Free energy	KCl (kcal·mol^{-1})	NaCl (kcal·mol^{-1})	ΔΔG[b] (kcal·mol^{-1})
ΔG_{dimer}	-7.6 ± 0.3[c]	-7.2 ± 0.7[c]	-0.4 ± 0.8
ΔG_{int}	-11.7 ± 0.1	-12.6 ± 0.2	0.9 ± 0.2
ΔG_c	0.4 ± 0.4	-2.8 ± 0.1	3.2 ± 0.4

[a] Values previously published [23] and determined based on the relationship $\Delta G_i = -RT\ln(k_i)$.
[b] Free energy difference for each set of parameters.
[c] Free energy change for solution dimerization measured independently using sedimentation equilibrium [17,23].

Millimolar ion affinities may seem weak when compared to the micromolar or nanomolar affinities associated with PR dimerization and DNA binding [16,17,21,22,26]. However, this is comparable to intracellular M^+ concentration. Typical estimates place Na^+ concentration at 11–44 mM [27, *and references therein*] and K^+ concentration at 100–140 mM [28]. This suggests that any minor decrease in Na^+ concentration or slight increase of K^+ concentration within the cell should significantly and preferentially decrease PR-B cooperative interactions. (Whether in Na^+ or K^+, PR-A cooperative interactions remain minimal on promoters with architecture such as HRE_2.)

Intriguingly, the PR isoforms are known to regulate a number of genes encoding various ion pumps and channels [11]. In particular, the Na^+,K^+-ATPase β1 gene is directly and strongly regulated by PR-B. The promoter for this gene has been experimentally dissected and been shown to contain multiple response elements capable of interacting with members of the steroid receptor family including the glucocorticoid receptor [29] and PR (Connaghan and Bain, unpublished data). We speculate that PR isoforms may act as ion sensors capable of directly controlling Na^+,K^+, ATPase β1 gene expression via a self-regulated feedback loop — any aberrant changes in Na^+ concentration will be allosterically coupled to changes in cooperative stabilization, influencing promoter occupancy and therefore allowing PR-B to precisely control ATPase gene activity. Cellular studies are currently underway in order to test this hypothesis.

5. Extension to the remaining steroid receptors

Our results on the PR isoforms suggest a clear role for cooperativity in generating isoform-specific gene regulation. This led us to consider whether the remaining steroid receptors might also exhibit different promoter binding energetics, particularly at the level of cooperativity. In order to test this hypothesis, we expressed and highly purified full-length, human ER and GR. Both receptors were first analyzed using sedimentation equilibrium and sedimentation velocity under identical (NaCl) buffer conditions used for PR-A and PR-B. The studies allowed us to estimate the dimerization energetics of GR. ER self-association energetics were too strong to determine using the absorbance optics of the analytical ultracentrifuge; however, we were able to semiquantitatively estimate affinity by coupling size exclusion chromatography with immunoblot detection. Finally, we carried out quantitative footprinting of the HRE_2 promoter to determine the energetics of intrinsic DNA binding and cooperativity

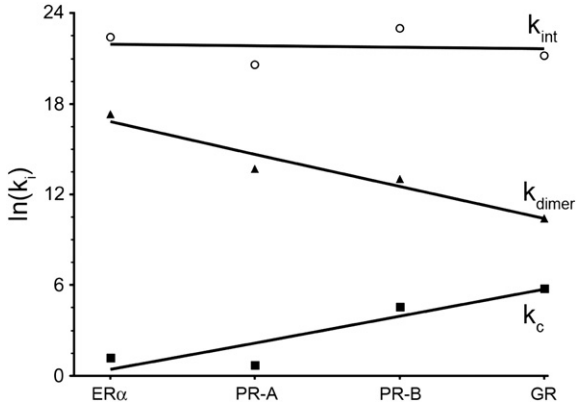

Fig. 8. Resolved binding parameters for receptor assembly at the HRE_2 promoter. Results are plotted as the natural log of each microstate constant, k_i. Symbols represent k_{int} (open circles), k_{dimer} (closed triangles), and k_c (closed squares). Each set of constants was fit to a straight line to emphasize the trend in the data.

for each receptor. Data were analyzed using the binding model shown in Fig. 2. The resolved parameters are plotted in Fig. 8.

It is evident that the intrinsic DNA binding affinity (k_{int}) is similar for all receptors. This is expected given the nearly identical crystallographic structure of the receptor DBDs. However, the dimerization energetics follow a linear slope, ranging from low nanomolar affinity for ER to supra-micromolar for GR. By contrast, the energetics of cooperativity follow an equal but opposite slope. Thus, dimerization and cooperativity appear to be compensating processes — receptors with weak dimerization energetics (and therefore primarily monomeric) are capable of strong cooperativity, whereas receptors with strong dimerization energetics achieve this at the cost of cooperativity.

The results of Fig. 8 suggest a code for generating differential receptor occupancies on different promoter architectures, even when all receptors are present at identical concentrations and are competing for the same binding sites. For example, promoters composed of largely palindromic response elements should be preferentially bound by ER (or receptors with ER-like energetics) due to its strong dimerization energetics. Conversely, promoters containing only half-site response elements should be occupied predominantly by GR, followed by PR-B and PR-A. Promoters containing a mix of palindromes and half-sites should be predominantly occupied by the PR isoforms.

We speculate that the ability of natural selection to generate steroid-specific gene regulation was coincident with the appearance of cooperativity. Yet cooperativity had to have been "paid for" by a decrease in dimerization energetics, since highly cooperative receptors would otherwise outcompete their non-cooperative counterparts for promoter binding. This also suggests that cooperativity and dimerization are somehow mechanistically linked.

6. Prostate derived factor (PDF) — the biology

To demonstrate the general utility of applying thermodynamic approaches toward an understanding of macromolecular structure and function, we analyzed a divergent member of the TGF-β superfamily, PDF. The TGF-β superfamily comprises a large number of secreted cytokines, which control a variety of physiological processes in cellular and organismal homeostasis. Importantly, TGF-β family members have been strongly implicated in cancer. For example, TGF-β1 exerts anti-proliferative functions in early stages of oncogenesis yet becomes tumor-promoting during the late stages of disease [30]. Thus, an understanding of TGF-β, and TGF-β-like molecules, is critical to our understanding of cancer biology.

Extensive *in vitro* and *in vivo* studies provide evidence for a critical role of PDF in tumor suppression. For example, transgenic mice with ubiquitous expression of PDF display reduced incidence of neoplasia in mouse models of lung and colon cancer [31,32]. Several reports indicate that PDF inhibits prostate cancer cell growth and induces apoptosis (reviewed in [33]). We have shown that forced expression of PDF inhibited proliferation and growth of xenografted tumors in PC-3 prostate cancer cells [34]. Additional support for a role of PDF in prostate cancer etiology derives from genetic studies. Genetic linkage analyses provide evidence of an association of the genomic locus containing the PDF gene in families with hereditary prostate cancer [35,36].

Much of the work carried out on TGF-β family members has focused on structural and functional studies — the biophysical aspects

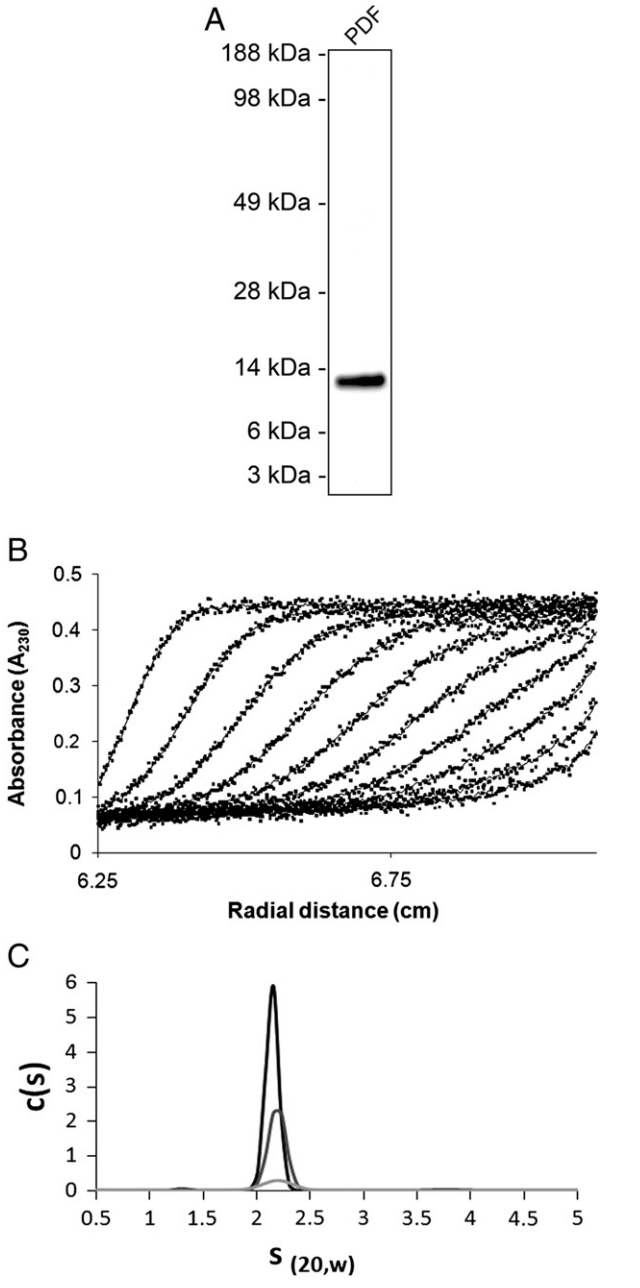

Fig. 9. Purification and sedimentation velocity analysis of PDF. (A) 1 μg PDF was resolved by SDS-PAGE and imaged by silver staining. (B) Representative sedimentation velocity data collected at 50,000 rpm. Only every thirtieth scan is shown for clarity. Buffer conditions were 5 mM HCl, 4 °C. (C) c(s) distributions for PDF at 40 μM (black line), 24 μM (dark gray) and 5 μM (light gray). Distributions were determined using SedFit [38].

have not been extensively investigated. In particular, little is known regarding the hydrodynamics of PDF. However, because it possesses the seven conserved cysteine residues thought to form a disulfide-linked "cysteine knot", a hallmark of TGF-β family members [37], it is proposed to assume a structure analogous to TGF-β. Nonetheless, PDF is a poorly conserved and distant member of the TGF-β family. Here we apply thermodynamic analysis analogous to those described above for steroid receptors, to investigate the biophysical properties of PDF. Specifically, we examined hydrodynamic properties of PDF as a step towards determining the structural characteristics of this critical regulator of cell signaling.

7. Hydrodynamic analysis of PDF

PDF was obtained from SBH Sciences (Natick, MA). Protein purity was determined by SDS-PAGE followed by silver staining (Fig. 9A). PDF was subjected to sedimentation velocity analysis to estimate assembly state and extent of structural homogeneity. Data was collected at multiple concentrations, ranging from 0.5 to 40 μM. A representative data set is shown in Fig. 9B. Data were analyzed using the program SedFit [38] to determine the sedimentation coefficient and average molecular weight at each concentration.

As seen in Fig. 9C, PDF sediments as a single peak of 2.28 s. The estimated molecular weight (25,479 Da) was consistent with that of a PDF dimer (25,029 Da (Table 3)). The lack of concentration dependence to the sedimentation coefficient distribution strongly supports the presence of a highly stable dimer, consistent with biochemical analyses of other TGF-β family members. When modeled as a prolate ellipsoid, the calculated frictional ratio yields an axial ratio of 5.2:1, again qualitatively similar to structural analyses [39].

However, a quantitative comparison of the experimental values for PDF to those calculated based on a representative TGF-β family member, Bone Morphogenetic Protein-6 [39], reveals considerable differences. This is most evident by comparing the experimentally determined sedimentation coefficient ($s_{20,w}$) of 2.28 s to the predicted value of 2.80 s as determined using HydroPro [40,41]. This difference is unlikely to be due to nonideality since there is no inverse concentration dependence to the sedimentation coefficient. Nor is this due to an inaccurate estimate of partial specific volume, since there is no evidence that mature PDF is post-translationally modified. Finally, this is not a consequence of buffer conditions, since an identical $s_{20,w}$ was obtained from pH 2 to 7.

This discrepancy could be explained by several possibilities. First, it is conceivable that the overall quaternary arrangement of PDF is different in solution than in the crystal lattice. Noting the importance of the cysteine knot and that NMR and crystal structures reveal generally similar folds, this seems unlikely. More likely is that the unstructured N-terminal and C-terminal residues not seen in the structural analyses impart significant hydrodynamic drag. It is also conceivable that the poorly conserved sequence composition of PDF results in a perturbation of tertiary structure. In any case, more detailed studies of PDF will be necessary to determine the parameters responsible for the observed differences. Finally, the results point out the limitations of visual inspection of macromolecular structure, and highlight the unique insight afforded to hydrodynamic and thermodynamic analyses.

Table 3
Hydrodynamic properties for PDF as determined by sedimentation velocity.

	PDF
$s_{20,w}$	2.28
f (g/s)	5.29×10^{-8}
f/f_0	1.26
Axial ratio	5.2:1
M_r (Da)	25,479

8. Conclusions and future directions

These studies reveal a number of findings that could not have been determined (and perhaps not even anticipated) from more traditional biochemical or structural approaches: the progesterone receptor isoforms maintain large differences in cooperative binding energetics; these differences can be modulated by physiological changes in solution conditions and promoter architecture; differences in cooperativity appear to be a common phenomenon for the steroid receptor family; across the family, changes in cooperativity are compensated for by changes in dimerization energetics. With regard to PDF, hydrodynamic results clearly indicate structural behavior not visible from high-resolution structural analysis. The challenge is now to understand more precisely how macromolecular energetics and hydrodynamics translate into cellular function.

Acknowledgments

This work was supported by NIH grants DK61933, DK88843 and a grant from the Avon Foundation for Women (DLB). We also thank Dr. Aaron F. Henegan for assistance with data collection and analysis.

References

[1] J. Abbott, D. Beckett, Cooperative binding of the *Escherichia coli* repressor of biotin biosynthesis to the biotin operator sequence, Biochemistry 32 (1993) 9649–9656.
[2] L.T. Perini, E.A. Doherty, E. Werner, D.F. Senear, Multiple specific CytR binding sites at the *Escherichia coli* deoP2 promoter mediate both cooperative and competitive interactions between CytR and cAMP receptor protein, J. Biol. Chem. 271 (1996) 33242–33255.
[3] V. Petri, M. Hsieh, M. Brenowitz, Thermodynamic and kinetic characterization of the binding of the TATA binding protein to the adenovirus E4 promoter, Biochemistry 34 (2002) 9977–9984.
[4] G.K. Ackers, A.D. Johnson, M.A. Shea, Quantitative model for gene regulation by λ phage repressor, Proc. Natl. Acad. Sci. U. S. A. 79 (1982) 1129–1133.
[5] G.K. Ackers, D.W. Bolen, The Gibbs conference on biothermodynamics: origins and evolution, Biophys. Chem. 64 (1997) 3–5.
[6] M.J. Tsai, B.W. O'Malley, Molecular mechanisms of action of steroid/thyroid receptor superfamily members, Annu. Rev. Biochem. 63 (1994) 451–486.
[7] P.H. Giangrande, A.E. Kimbrel, D.P. Edwards, D.P. McDonnell, The opposing transcriptional activities of the two isoforms of the human progesterone receptor are due to differential cofactor binding, Mol. Cell. Biol. 20 (2000) 3102–3115.
[8] X. Li, J. Wong, S.Y. Tsai, M.-J. Tsai, B.W. O'Malley, Progesterone and glucocorticoid receptors recruit distinct coactivator complexes and promote distinct patterns of local chromatin modification, Mol. Cell. Biol. 23 (2003) 3763–3773.
[9] S.H. Meijsing, M.A. Pufall, A.Y. So, D.L. Bates, L. Chen, K.R. Yamamoto, DNA binding site sequence directs glucocorticoid receptor structure and activity, Science 324 (2009) 407–410.
[10] N.J. McKenna, B.W. O'Malley, Combinatorial control of gene expression by nuclear receptors and coregulators, Cell 108 (2002) 465–474.
[11] J.K. Richer, B.M. Jacobsen, N.G. Manning, M.G. Abel, D.M. Wolf, K.B. Horwitz, Differential gene regulation by the two progesterone receptor isoforms in human breast cancer cells, J. Biol. Chem. 277 (2002) 5209–5218.
[12] Y. Wan, S.K. Nordeen, Overlapping but distinct gene regulation profiles by glucocorticoids and progestins in human breast cancer cells, Mol. Endocrinol. 16 (2002) 1204–1214.
[13] D.G. Monroe, B.J. Getz, S.A. Johnsen, B.L. Riggs, S. Khosla, T.C. Spelsberg, Estrogen receptor isoform-specific regulation of endogenous gene expression in human osteoblastic cell lines expressing either ERα or ERβ, J. Cell. Biochem. 90 (2003) 315–326.
[14] P.A. Mote, S. Bartow, N. Tran, C.L. Clarke, Loss of co-ordinate expression of progesterone receptors A and B is an early event in breast carcinogenesis, Breast Cancer Res. Treat. 72 (2002) 163–172.
[15] T.A. Hopp, H.L. Weiss, S.G. Hilsenbeck, Y. Cui, D.C. Alfred, K.B. Horwitz, S.A. Fuqua, Breast cancer patients with progesterone receptor PR-A-rich tumors have poorer disease-free survival rates, Clin. Cancer Res. 15 (2004) 2751–2760.
[16] K.D. Connaghan-Jones, A.F. Heneghan, M.T. Miura, D.L. Bain, Hydrodynamic analysis of the human progesterone receptor A-isoform reveals that self-association occurs in the micromolar range, Biochemistry 45 (2006) 12090–12099.
[17] A.F. Heneghan, N. Berton, M.T. Miura, D.L. Bain, Self-association energetics of an intact, full-length nuclear receptor: the B-isoform of human progesterone receptor dimerizes in the micromolar range, Biochemistry 44 (2005) 9528–9537.
[18] M. Brenowitz, D.F. Senear, M.A. Shea, G.K. Ackers, Footprint titrations yield valid thermodynamic isotherms, Proc. Natl. Acad. Sci. U. S. A. 83 (1986) 8462–8466.
[19] T.L. Hill, An Introduction to Statistical Thermodynamics, Dover Publications, New York, 1960.
[20] A.F. Heneghan, K.D. Connaghan-Jones, M.T. Miura, D.L. Bain, Coactivator assembly at the promoter: efficient recruitment of SRC2 is coupled to cooperative DNA binding by the progesterone receptor, Biochemistry 46 (2007) 11023–11032.

[21] K.D. Connaghan-Jones, A.F. Heneghan, M.T. Miura, D.L. Bain, Thermodynamic analysis of progesterone receptor–promoter interactions reveals a molecular model for isoform-specific function, Proc. Natl. Acad. Sci. U. S. A. 104 (2007) 2187–2192.
[22] K.D. Connaghan-Jones, A.F. Heneghan, M.T. Miura, D.L. Bain, Thermodynamic dissection of progesterone receptor interactions at the mouse mammary tumor virus promoter: monomer binding and strong cooperativity dominate the assembly reaction, J. Mol. Biol. 377 (2008) 1144–1160.
[23] K.D. Connaghan, A.F. Heneghan, M.T. Miura, D.L. Bain, Na^+ and K^+ allosterically regulate cooperative DNA binding by the human progesterone receptor, Biochemistry 49 (2009) 422–431.
[24] G. Chalepakis, J. Arnemann, E. Slater, H.-J. Bruller, B. Gross, M. Beato, Differential gene activation by glucocorticoids and progestins through the hormone regulatory element of mouse mammary tumor virus, Cell 53 (1988) 371–382.
[25] T. Perlmann, P. Eriksson, O. Wrange, Quantitative analysis of the glucocorticoid receptor–DNA interaction at the mouse mammary tumor virus glucocorticoid response element, J. Biol. Chem. 265 (1990) 17222–17229.
[26] A.F. Heneghan, K.D. Connaghan-Jones, M.T. Miura, D.L. Bain, Cooperative DNA binding by the B-isoform of human progesterone receptor: thermodynamic analysis reveals strongly favorable and unfavorable contributions to assembly, Biochemistry 45 (2006) 3285–3296.
[27] S.R. Gullans, M.J. Avison, T. Ogino, G. Giebisch, R.G. Shulman, NMR measurements of intracellular sodium in the rabbit proximal tubule, Am. J. Physiol. Renal Physiol. 249 (1985) F160–F168.
[28] B. László, M. Teréz, E. Miklós, K. Zoltán, T. Lajos, Flow cytometric determination of intracellular free potassium concentration, Cytometry 28 (1997) 42–49.
[29] A. Derfoul, N.M. Robertson, J.B. Lingrel, D.J. Hall, G. Litwack, Regulation of the human Na/K-ATPase beta 1 gene promoter by mineralocorticoid and glucocorticoid receptors, J. Biol. Chem. 273 (1998) 20702–20711.
[30] A.B. Roberts, L.M. Wakefield, The two faces of transforming growth factor β in carcinogenesis, Proc. Natl. Acad. Sci. U. S. A. 100 (2003) 8621–8623.
[31] S.J. Baek, R. Okazaki, S.-H. Lee, J. Martinez, J.-S. Kim, K. Yamaguchi, Y. Mishina, D.W. Martin, A. Shoieb, M.F. McEntee, T.E. Eling, Nonsteroidal anti-inflammatory drug-activated gene-1 over-expression in transgenic mice suppresses intestinal neoplasia, Gastroenterology 131 (2006) 1553–1560.
[32] M. Cekanova, S.-H. Lee, R.L. Donnell, M. Sukhthankar, T.E. Eling, S.M. Fischer, S.J. Baek, Nonsteroidal anti-inflammatory drug-activated gene-1 expression inhibits urethane-induced pulmonary tumorigenesis in transgenic mice, Cancer Prev. Res. 2 (2009) 450–458.
[33] T.E. Eling, S.J. Baek, M. Shim, C.H. Lee, NSAID activated gene (NAG-1), a modulator of tumorigenesis, J. Biochem. Mol. Biol. 39 (2006) 649–655.
[34] J.R. Lambert, J.A. Kelly, M. Shim, W.E. Huffer, S.K. Nordeen, S.J. Baek, T.E. Eling, M.S. Lucia, Prostate derived factor in human prostate cancer cells: gene induction by vitamin D via a p53-dependent mechanism and inhibition of prostate cancer cell growth, J. Cell. Physiol. 208 (2006) 566–574.
[35] C.-L. Hsieh, I. Oakley-Girvan, R.R. Balise, J. Halpern, R.P. Gallagher, A.H. Wu, L.N. Kolonel, L.E. O'Brien, I.G. Lin, D.J. Van Den Berg, C.-Z. Teh, D.W. West, A.S. Whittemore, A genome screen of families with multiple cases of prostate cancer: evidence of genetic heterogeneity, Am. J. Hum. Genet. 69 (2001) 148–158.
[36] F. Wiklund, E.M. Gillanders, J.A. Albertus, A. Bergh, J.-E. Damber, M. Emanuelsson, D.L. Freas-Lutz, D.E. Gildea, I. Göransson, M.S. Jones, B.-A. Jonsson, F. Lindmark, C.J. Markey, E.L. Riedesel, E. Stenman, J.M. Trent, H. Grönberg, Genome-wide scan of Swedish families with hereditary prostate cancer: suggestive evidence of linkage at 5q11.2 and 19p13.3, Prostate 57 (2003) 290–297.
[37] M. Böttner, M. Laaff, B. Schechinger, G. Rappold, K. Unsicker, C. Suter-Crazzolara, Characterization of the rat, mouse, and human genes of growth/differentiation factor-15/macrophage inhibiting cytokine-1 (GDF-15/MIC-1), Gene 237 (1999) 105–111.
[38] P. Schuck, On the analysis of protein self-association by sedimentation velocity analytical ultracentrifugation, Anal. Biochem. 320 (2003) 104–124.
[39] G.P. Allendorph, M.J. Isaacs, Y. Kawakami, J.C. Izpisua Belmonte, S. Choe, BMP-3 and BMP-6 structures illuminate the nature of binding specificity with receptors, Biochemistry 46 (2007) 12238–12247.
[40] J. García de la Torre, M.L. Huertas, B. Carrasco, Calculation of hydrodynamic properties of globular proteins from their atomic-level structure, Biophys. J. 78 (2000) 719–730.
[41] J. Garcia de la Torre, S. Navarro, M.C. Lopez Martinez, F.G. Diaz, J.J. Lopez Cascales, HYDRO: a computer program for the prediction of hydrodynamic properties of macromolecules, Biophys. J. 67 (1994) 530–531.
[42] M.L. Johnson, J.J. Correia, D.A. Yphantis, H.R. Halvorson, Analysis of data from the analytical ultracentrifuge by nonlinear least-squares techniques, Biophys. J. 36 (1981) 575–588.
[43] G. Theofan, A.C. Notides, Characterization of the calf uterine progesterone receptor and its stabilization by nucleic acids, Endocrinology 114 (1984) 1173–1179.
[44] J.S. Philo, A method for directly fitting the time derivative of sedimentation velocity data and an alternative algorithm for calculating sedimentation coefficient distribution functions, Anal. Biochem. 279 (2000) 151–163.
[45] W.F. Stafford, Boundary analysis in sedimentation transport experiments: a procedure for obtaining sedimentation coefficient distributions using the time derivative of the concentration profile, Anal. Biochem. 203 (1992) 295–301.